

ARMY RESEARCH LABORATORY



Simulating Photonic Band Gaps in Crystals

by Daniel H. Kodan and Peter W. Chung

ARL-TR-4167

June 2007

NOTICES

Disclaimers

The findings in this report are not to be construed as an official Department of the Army position unless so designated by other authorized documents.

Citation of manufacturer's or trade names does not constitute an official endorsement or approval of the use thereof.

DESTRUCTION NOTICE—Destroy this report when it is no longer needed. Do not return it to the originator.

Army Research Laboratory

Aberdeen Proving Ground, MD 21005-5066

ARL-TR-4167

June 2007

Simulating Photonic Band Gaps in Crystals

by Daniel H. Kodan and Peter W. Chung
Computational and Information Sciences Directorate, ARL

REPORT DOCUMENTATION PAGE				Form Approved OMB No. 0704-0188	
<p>Public reporting burden for this collection of information is estimated to average 1 hour per response, including the time for reviewing instructions, searching existing data sources, gathering and maintaining the data needed, and completing and reviewing the collection information. Send comments regarding this burden estimate or any other aspect of this collection of information, including suggestions for reducing the burden, to Department of Defense, Washington Headquarters Services, Directorate for Information Operations and Reports (0704-0188), 1215 Jefferson Davis Highway, Suite 1204, Arlington, VA 22202-4302. Respondents should be aware that notwithstanding any other provision of law, no person shall be subject to any penalty for failing to comply with a collection of information if it does not display a currently valid OMB control number.</p> <p>PLEASE DO NOT RETURN YOUR FORM TO THE ABOVE ADDRESS.</p>					
1. REPORT DATE (DD-MM-YYYY)	2. REPORT TYPE		3. DATES COVERED (From - To)		
June 2007	Final		July 2006 to May 2007		
4. TITLE AND SUBTITLE			5a. CONTRACT NUMBER		
Simulating Photonic Band Gaps in Crystals			5b. GRANT NUMBER		
			5c. PROGRAM ELEMENT NUMBER		
6. AUTHOR(S)			5d. PROJECT NUMBER		
Daniel H. Kodan and Peter W. Chung (both of ARL)			7UH7CL		
			5e. TASK NUMBER		
			5f. WORK UNIT NUMBER		
7. PERFORMING ORGANIZATION NAME(S) AND ADDRESS(ES)			8. PERFORMING ORGANIZATION REPORT NUMBER		
U.S. Army Research Laboratory Computational and Information Sciences Directorate Aberdeen Proving Ground, MD 21005-5066			ARL-TR-4167		
9. SPONSORING/MONITORING AGENCY NAME(S) AND ADDRESS(ES)			10. SPONSOR/MONITOR'S ACRONYM(S)		
			11. SPONSOR/MONITOR'S REPORT NUMBER(S)		
12. DISTRIBUTION/AVAILABILITY STATEMENT Approved for public release; distribution is unlimited.					
13. SUPPLEMENTARY NOTES					
14. ABSTRACT <p>This report summarizes the progress and results for a Student Temporary Employment Program Internship from July 2006 through June 2007. The report presents an introduction to the concept of photonic crystals through quantitative calculations of band gaps with the use of an open source code. Photonics is the science and technology of generating, controlling, and detecting photons, particularly in the visible light and near infrared spectrum.</p> <p>The first part of the report provides a detailed introduction to the principle of photonics from an engineering perspective and discusses possible concepts and applications for the future. Sample calculations for phonon dispersion curves are then presented with the use of simplified models of crystals to demonstrate universal principles of vibrational behavior to understand the properties of crystals. To this end, a MATLAB¹ program was written to generate dispersion relations for two types of reduced dimensional lattices.</p> <p>The second part of the report demonstrates the implementation of a photonic band gap model. The calculations were performed with the use of the Massachusetts Institute of Technology photonic band gap code (MPB). The code was compiled and built on the computers at the U.S. Army Research Laboratory's Major Shared Resource Center, and results verifying the installation are shown.</p> <p>The report concludes with appendices detailing MATLAB code for the phonon calculations, input decks for MPB, and an ancillary literature review of ferroelectric fatigue in crystals, which was another topic of interest early in the internship.</p>					
15. SUBJECT TERMS band gap; crystals; modeling; photonics					
16. SECURITY CLASSIFICATION OF:			17. LIMITATION OF ABSTRACT	18. NUMBER OF PAGES	19a. NAME OF RESPONSIBLE PERSON Daniel H. Kodan
a. REPORT Unclassified	b. ABSTRACT Unclassified	c. THIS PAGE Unclassified	SAR	50	19b. TELEPHONE NUMBER (Include area code) 410-278-6027

Contents

List of Figures	iv
Acknowledgments	v
1. Background	1
2. Photonic Crystals	2
3. Photonic Crystal Applications	4
4. Dispersion Curve MATLAB Program	7
4.1 Normal Modes of a One-Dimensional Monatomic Bravais Lattice.....	8
4.2 Normal Modes of a One-Dimensional Lattice with a Basis.....	11
4.3 One-Dimensional MATLAB Results	12
4.4 Normal Modes of a Two-Dimensional Monatomic Lattice	14
4.5 Two-Dimensional MATLAB Results	16
5. Massachusetts Institute of Technology (MIT) Photonic Bands	17
5.1 Diamond Structure	19
5.2 Tri-rods Structure	21
5.3 Sample Structure	23
5.4 MIT Photonic-Bands Conclusion.....	25
7. References	26
Appendix A. Lennard-Jones Potential	27
Appendix B. MATLAB Code: Dispersion Curves for One-Dimensional Lattice	29
Appendix C. MATLAB Code: Two-Dimensional Phonon Dispersion Curve	31
Appendix D. Diamond Structure Control File (diamond.ctl)	33
Appendix E. Tri-Rods Structure Control File (tri-rods.ctl)	35
Appendix F. An Introduction to Ferroelectric Fatigue	37
Distribution List	42

List of Figures

Figure 1. Depiction of sample photonic band gap	2
Figure 2. Simplified representation of one-, two-, and three-dimensional crystals (4)	3
Figure 3. Sample of actual 3-D photonic band gap crystal structures (Φ gives the filling fraction or percentage of unit cell occupied by material [5]).....	3
Figure 4. Yablonovite	4
Figure 5. Schematic of simulation test setup (8).....	5
Figure 6. Schematic of typical NPC sensor response from simulation.....	5
Figure 7. Schematic of flexible photonic crystal	6
Figure 8. Refraction angle attributable to elongation (9).....	6
Figure 9. Strain on a crystalline silicon: (a) crystalline silicon waveguide on an SOI wafer; (b) wave guide with a deposited straining layer (10).....	7
Figure 10. Representation of a 1-D chain (12).	9
Figure 11. Representation of a 1-D chain with a basis (11).....	11
Figure 12. Dispersion curve for a 1-D chain with a basis.....	13
Figure 13. Dispersion curve for a monatomic 1-D chain.....	13
Figure 14. Ion motion during different vibration modes (12).....	14
Figure 15. Representation of a 2-D monatomic lattice.....	15
Figure 16. Dispersion curve for a 2-D lattice	16
Figure 17. Dispersion curve for a 2-D lattice	17
Figure 18. Diamond structure depiction (13) (MIT photonic-band tutorial figure).	20
Figure 19. Diamond band diagram (14) (MIT photonic-band tutorial figure).	20
Figure 20. Diamond band diagram (MIT photonic-band program generated plot).....	21
Figure 21. Rods in a triangular lattice (13), top view.	21
Figure 22. Tri-rods band diagram (13) (MIT photonic band tutorial figure).....	22
Figure 23. Tri-rods band diagram (MIT photonic band program-generated plot).....	23
Figure 24. Sample control file for MPB.	24
Figure 25. Sample band structure (MIT photonic band program-generated plot).....	24
Figure A-1. Lennard-Jones potential	28

Acknowledgments

The authors gratefully acknowledge partial support from the U.S. Army Research Laboratory's Major Shared Resource Center at the Computational & Informational Sciences Directorate, High Performance Computing Division, Computational Sciences & Engineering Branch through the Student Temporary Employment Program. Partial support is also gratefully acknowledged through the Joint Science and Technology Office of the Defense Threat Reduction Agency.

INTENTIONALLY LEFT BLANK

1. Background

Photonics is the study of the creation, control, and detection of photons. The topic is of increasing interest because of projected value in new types of sensor and computing devices. As more is learned about the field and its applications, the larger the support for the research becomes. It is closely related to quantum optics and optoelectronics. Quantum optics refer to the principal research, while photonics focus on the application of the technology (1). Opto-electronics is the emerging field of light-driven (photon flow) electronics as opposed to the conventional electrically driven (electron flow) electronics.

The basis of photonics is the photon¹. The modern definition of the photon was developed by Albert Einstein during the early 1900s. He originally called them “light quanta”. They were first referred to as photons by the chemist Gilbert N. Lewis in 1926. He based the name on the Greek word “phos” meaning light (1). A photon is the most basic electromagnetic component. The photon is a quanta or “packet” of electromagnetic energy that exhibits particle-like and wave-like characteristics. A photon is represented by γ or as the product hv , h being Planck’s constant and v , the frequency of the electromagnetic wave. The momentum of a photon is calculated as hv/c , c being the speed of light which is the constant velocity of all photons. Photons are massless and have no electric charge. Photons are created during several circumstances (1):

1. A charged particle undergoes acceleration;
2. An atomic particle drops from a higher to lower energy state;
3. An atomic particle is destroyed.

The field of photonics began with the invention of the laser in 1960 by Theodore Maiman at Hughes Research Laboratories. The field began to expand with the discovery of the optical fiber in 1970. The optical fiber functioned as a medium for the transmission of light (1). The optical fiber allowed for the controlling of photon flows.

The wave-particle duality of light is a crucial concept in the field of photonics. Einstein developed photons to explain his experiments which showed that light did not follow the classical wave model. This model depicts light as a wave that propagates through a medium accordingly. These wave models explain the refraction, diffraction, and interference of light since they are wave behaviors. On the other hand, experiments show that photons do not spread as they propagate and they do not split as waves do. These are particle-like behaviors. This comes to the duality principle that the photon particles produce the wave-like electromagnetic field. These characteristics of light are important factors in the research and application of photonics.

¹A photon is a unit of intensity of light at the retina equal to the illumination received per square millimeter of a pupillary area from a surface having a brightness of one candle per square meter.

2. Photonic Crystals

Photonic crystals are periodic material structures that affect the motion of photons propagating through them. They affect photons in the same way a semiconductor crystal affects the motion of electrons. The crystals consist of periodic dielectric structures that affect electromagnetic wave propagation. A dielectric is a substance that resists electric current, meaning it acts as an electrical insulator. In some instances, a lack of substance or vacancy can act as a dielectric (e.g., air). The photonic crystals affect propagation by allowing electromagnetic waves of certain wavelengths to pass while blocking others. A range of blocked wavelengths is called a photonic band gap (shown in yellow in figure 1). There are some naturally occurring photonic crystals such as the gemstone opal and the substance that comprises butterfly wings (2).

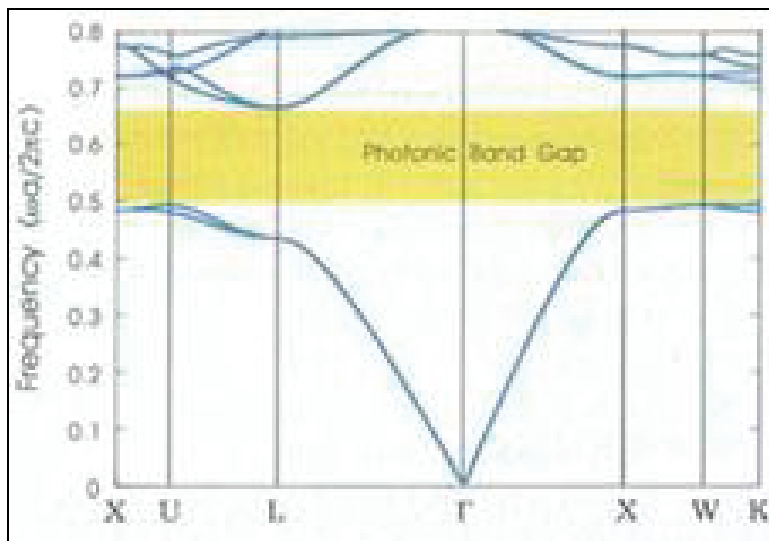


Figure 1. Depiction of sample photonic band gap. (Yellow shaded region shows a photonic band gap on a photonic band diagram. The letters along x axis represent the different directions along the crystal lattice [3].)

Diffraction is the basic principle behind the photonic crystal function. Diffraction refers to different wave propagation characteristics such as bending, spreading, and interference. Diffraction effects occur most when the wavelength and affecting medium structure are on the same scale (2). The visible spectrum occurs on the 400- to 700-nm wavelength scale. As a result, the feature periodicity of the photonic crystals must also exist on this scale.

Photonic crystals can affect propagation in one, two, and three dimensions, as shown in figure 2. The periodic structure and dielectric nature of the crystal determine its ability to produce a band gap. Lord Rayleigh was the first scientist to study the propagation of electromagnetic waves in periodic structured media in 1887 (2). He studied the reflective properties of a crystalline mineral

that corresponded to a one-dimensional (1-D) photonic crystal. He observed a small band gap through which light could not propagate through the planes of the crystal.

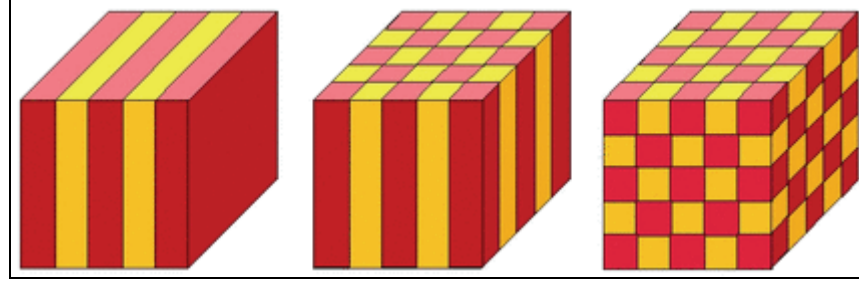


Figure 2. Simplified representation of one-, two-, and three-dimensional crystals (4).

Photonic crystals possess two types of polarizations by symmetry: the transverse magnetic (TM) in which the electric and magnetic fields are orthogonal to one another, and the transverse electric (TE) in which the electric and magnetic fields are in the same plane. By judicious placement of materials with different high and low indices inside an area or volume, hypothetical TE and TM band gap materials may be created. Using this simple principle, one can construct a potentially infinite number of variations in the topology of constituents to create photonic materials of varying properties, as in figure 3.

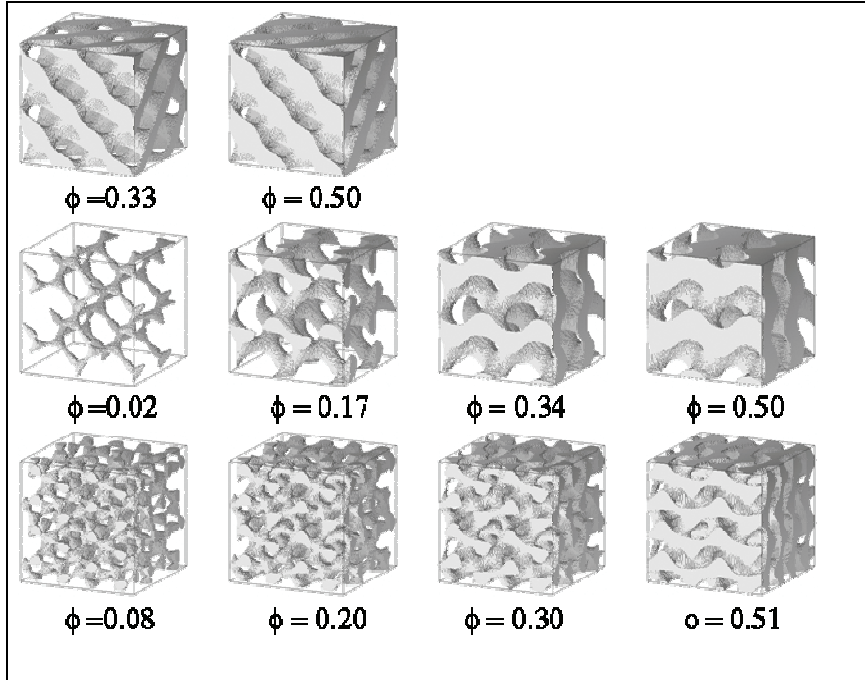


Figure 3. Sample of actual 3-D photonic band gap crystal structures (Φ gives the filling fraction or percentage of unit cell occupied by material [5]).

Eli Yablonovitch and Sajeev John both submitted independent papers on the photonic band gap in 1987, and the search for multi-dimensional band gap crystals began (6). Yablonovitch fabricated

the first 3-D photonic band gap crystal while working for Bell Communications Research in 1991 (6). The material was composed of silicon and silicon dioxide arranged in a diamond tetrahedral structure. The structure is now known as yablonovite (see figure 4). Since their discovery, 3-D band gaps have been demonstrated in simple cubic and face-centered cubic structures as well.

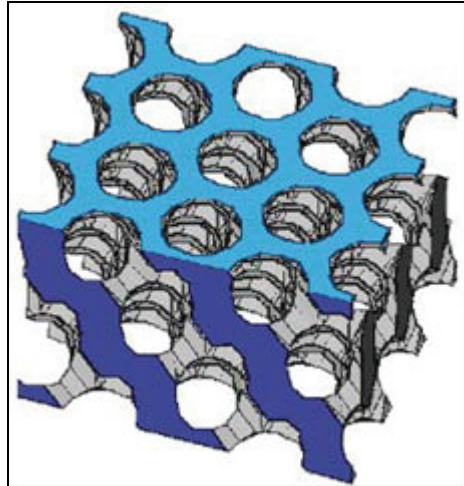


Figure 4. Yablonovite. (This was the first 3-D crystal with a band gap that was created when holes were drilled into a ceramic material [7].)

3. Photonic Crystal Applications

The potential application of photonic crystals in emerging technologies is very extensive. The volume of photonics research has already produced many new developments in the control of electromagnetic waves. One-dimensional photonic crystals are currently used in thin-film optic applications. They are also being used to form reflective layers on mirrors and lenses and to create color-changing inks and paints. Two-dimensional photonic crystal fibers are produced by several companies to transmit and control light in frequencies that conventional fiber optics fail to transmit (6). Three-dimensional photonic crystals are much more difficult to fabricate and as a result, have not yet been mass produced or applied to commercial products (4).

An exploratory simulation was done to explore the use of nano photonic sensors for micro-damage detection (8). El-Kady and Reha Taha demonstrated a simulation model that is comprised of a nano photonic sensor (NPC) attached to a composite bar. When damage is created in the composite bar, the photonic sensor's band gap profile experiences a significant change. The schematic showing this proposed setup is presented in figure 5. A slight change in the NPC's surroundings (damage in the composite bar) will result in a change in the crystal's dimensions. As the crystal's dimensions change, so do its optical properties (8). We can use the NPC to quantify damage in the composite

bar by monitoring the NPC's optical response before and after damage is induced in the bar. The simulation resulted in a theoretically verified damage metric (Nano Spectrum Index) that can be extracted from the frequency domain response of the NPC sensor, as seen in figure 6 (8). The simulation will hopefully lead to the development of NPC sensors that will allow for damage detection at nano scales, which is currently unattainable with contemporary sensors.

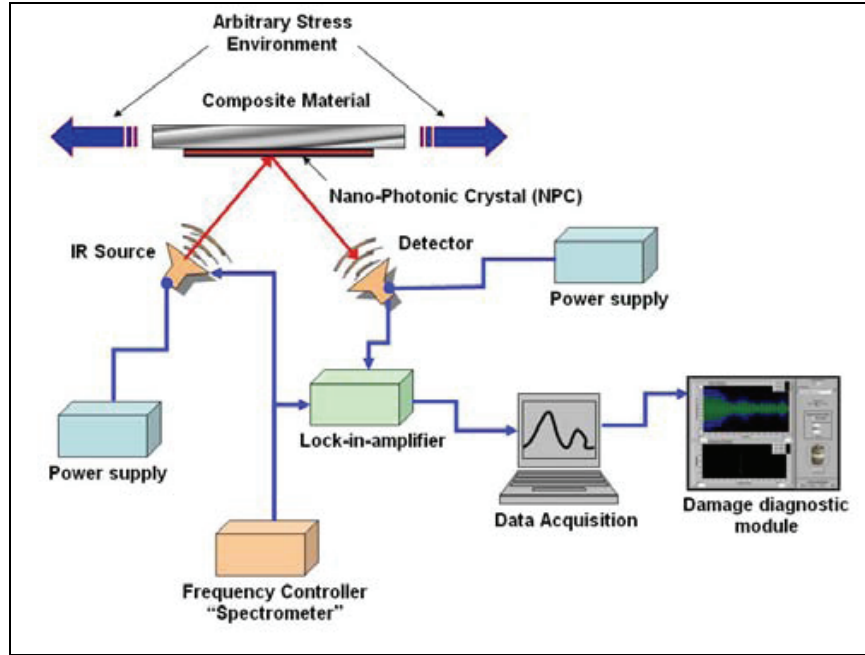


Figure 5. Schematic of simulation test setup (8).

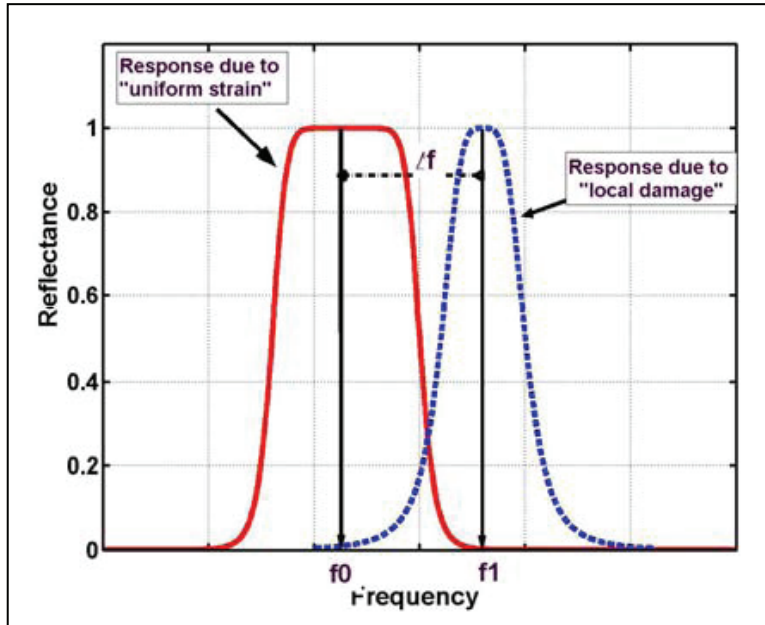


Figure 6. Schematic of typical NPC sensor response from simulation.
(Frequency shift of NPC response is caused by local damage in the composite bar as a result of a non-uniform strain [8].)

Park and Lee (9) have theoretically investigated the effect of a mechanical stress applied to a photonic crystal. They report a flexible photonic crystal with a tunable band structure that is controlled through the use of a nano-/microelectromechanical system actuator (see figure 7). For the theoretical modeling, the photonic crystal structure consisted of a pattern of high-index dielectric material and a low-index flexible polymer (index referring to the refractive index of the material). With the large effect of physical change on the band structure of photonic crystals, a large range of tunability is possible (9). With elongations as small as 10% in the photonic crystal, a change in the refraction angle of an incident beam was as large as 75 degrees (9). Figure 8 shows the refraction angles for different elongations; these were calculated with the theoretically derived band structure. The sizable change in refraction angle attributable to applied mechanical stress shows promise for the use of photonic crystals as optical beam controlling devices. The goal of the research was to create a system that could control a photonic band structure in real time. With control over the optical properties of the photonic crystal, the crystals can act as optical switches, routers, and modulators on the nano-scale (9).

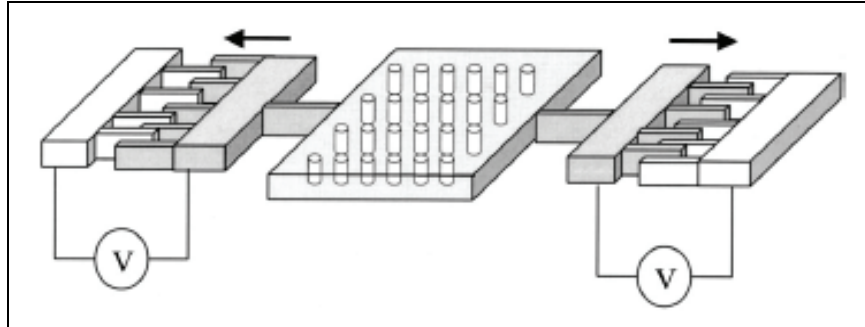


Figure 7. Schematic of flexible photonic crystal. (Mechanical stress is applied to the photonic crystals by micro-electro-mechanical sensors actuators on either side [9].)

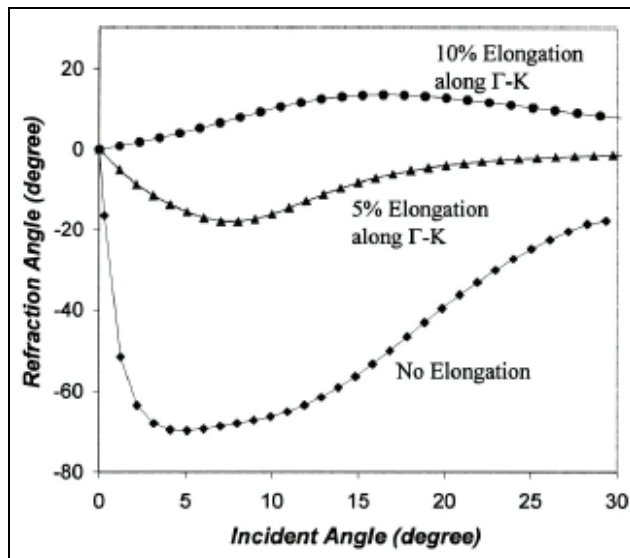


Figure 8. Refraction angle attributable to elongation (9).

Jacobsen experimentally found that a linear electro-optic effect can be realized in silicon by breaking the crystal symmetry. The crystal symmetry is broken through the use of a straining layer deposited on top of the silicon feature, e.g. wave guide (see figure 9). In silicon's natural state, its crystal symmetry prevents the existence of a linear electro-optic effect (10). As the silicon is strained, its bulk refractive index fluctuates in a linear fashion as a function of an externally applied electric field. The experiment was conducted when a silicon nitride glass straining layer was deposited on a silicon wave guide; the entire structure was on a silicon-on-insulator (SOI) wafer (10). Application of silicon as an opto-electronic material is a highly sought-after objective. This would allow for the creation of combination electronic and optic components composed entirely of silicon. The overall goal of the research is to eventually use a strain-induced electro-optic effect to replace the electronic bus in computers with an optical bus that performs at higher speeds (10).

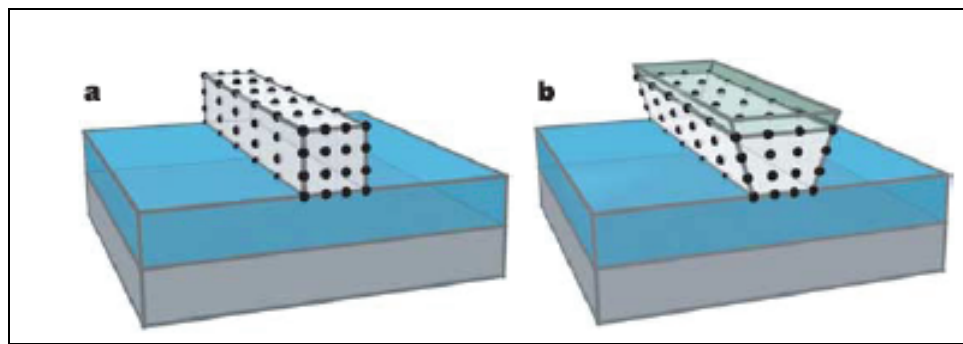


Figure 9. Strain on a crystalline silicon: (a) crystalline silicon waveguide on an SOI wafer; (b) wave guide with a deposited straining layer (10).

Many papers have recently been published, documenting the advances in the field. These advances will hopefully lead to commercialization of photonic crystals for advanced technologies. Most of the research is in its infancy and therefore, many are theoretical simulations and analytical explorations. As the field and technology advances, more of these applications will be attempted experimentally. The experiments will demonstrate whether the applications are commercially viable.

4. Dispersion Curve MATLAB² Program

With MATLAB, programs were written to compute the phonon dispersion curves for different materials. We adopted the use of phonons instead of photons for didactic demonstration of band gaps. The code driving the programs was written with Kittel's text (11) as a primary reference. The text explained the calculation of dispersion curves for 1-D crystal lattices with a monatomic structure as well as with a basis. After a code was written to display the dispersion curves for a 1-D

²MATLAB is a registered trademark of The MathWorks, <http://www.mathworks.com>.

crystal, the calculations were further expanded and a program was created to show the dispersion curves through a 2-D planar crystal lattice. The MATLAB program provides powerful graphing abilities that were well suited to simulating the dispersion curve calculations. The ensuing sections show the derivations behind the calculations, the program code, and sample output from the programs.

The phonon program is a good starting point for the further study of photonics. The calculation of the phonon dispersion curves is more pedagogically simplistic for understanding band gaps. The phonon program provides a foundation for the possible extension to graph photonic curves. The ability to graph the frequency at which electromagnetic energy quanta can pass through different crystal lattices is an invaluable tool. The graphs show the band gaps and they would be extremely useful for the manufacture and control of materials for photonics applications.

The following sections show the derivations of equations showing the frequency of vibration based on a wave vector k . These modes of vibration are known as phonons and they occur in structures with rigid crystal lattices (11). These phonon mode graphs are known as dispersion curves. The physical, such as thermal and conductive, properties of materials depend on these phonons.

The first derivation in section 4.1 is for the normal modes of a 1-D monatomic Bravais lattice. In a Bravais lattice, all the lattice points are the same. This by default means that the ions in the crystal are all the same kind, thus the monatomic label.

The derivation in section 4.2 is for the normal modes of a 1-D lattice with a basis. This is still a Bravais lattice because the basis is an identical ion.

Section 4.3 contains the derivation for the normal modes of a 2-D monatomic lattice. Instead of the 1-D chain, this derivation solves for the phonon modes of a 2-D planar crystal structure.

The next step would be to further develop the 2-D code to handle general crystal structures. This code would need to handle different crystal structures with different ions at lattice points or structures with ions that have a basis. After that is completed, a comprehensive code for a 3-D lattice could be formulated. This would increase the code's complexity immensely and would yield a powerful computational tool.

4.1 Normal Modes of a One-Dimensional Monatomic Bravais Lattice

Take a line of ions all of the same mass M spaced at an interval distance of a , as indicated in figure 10. This gives the 1-D Bravais lattice vectors as $\mathbf{R} = na$, where n is a counting integral. Assuming the line is envisioned in the horizontal direction, the displacement of a given ion from its equilibrium position is $u(na)$. The most basic way to view the chain of ions is as a spring-mass chain as seen in figure 10. This allows for the spring potential energy equation to represent the fundamental interaction between the ions.

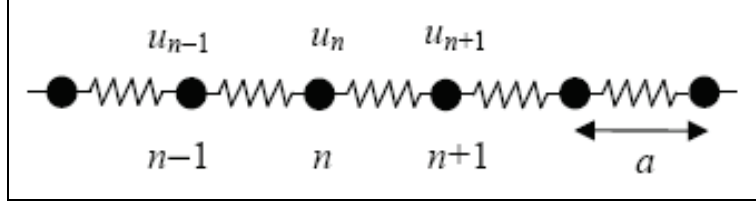


Figure 10. Representation of a 1-D chain (12).

$$U = \frac{1}{2} kx^2.$$

The potential energy U is equated to a function of the spring constant k and the ion displacement.

$$\begin{aligned} k &= K; \\ x &= [u(na) - u([n+1]a)]. \end{aligned}$$

The spring constant k is replaced with $K = \varphi''(a)$, where $\varphi(x)$ represents the interaction energy of two ions at distance x apart along the line (spring constant). This interaction energy is found with the Lennard-Jones potential described in appendix A. We find the displacement x by taking the displacement of the ion from equilibrium and subtracting the displacement of the next ion from its equilibrium. These substitutions give the harmonic potential energy equation as the summation over all ions in the chain:

$$U^{harm} = \frac{1}{2} K \sum_n [u(na) - u([n+1]a)]^2, \quad (1)$$

$$M\ddot{u}(na) = -\frac{\partial U^{harm}}{\partial u(na)} = -K[2u(na) - u([n-1]a) - u([n+1]a)]. \quad (2)$$

The equations of motion of the ions show the theoretical interaction of two neighboring ions connected by a perfect spring (11). We find the motion equation by taking the derivative of the harmonic potential energy with respect to the ion's displacement.

If the chain is considered a finite system with N ions, boundary conditions can be implemented to retrieve solutions from the motion equation. In order to apply boundary conditions, the finite chain must be viewed as a loop so the $N+1$ ion is the first ion of the chain (11). These boundary conditions are expressed mathematically as

$$u([N+1]a) = u(a); \quad u(0) = u(Na). \quad (3)$$

Solutions to the equation of motion in equation 2 take the form

$$u(na, t) \propto e^{i(kna - \omega t)}. \quad (4)$$

Applying the boundary conditions of equation 3 leads to the wave vector k equation to be

$$e^{ikNa} = 1; \quad k = \frac{2\pi}{a} \frac{n}{N}. \quad (5)$$

Only N values of k consistent with equation 5 yield distinct solutions, taken between $-\pi/a$ and π/a in order to view the dispersion curve about the zero wave vector. This range covers $2\pi/a$; any of the distinct solutions shifted by $2\pi/a$ will return the same result, meaning that this range produces the entire distinct dispersion curve.

Substituting the solutions of the form in equation 4 into the equation 2 of motion gives the following:

$$-M\omega^2 e^{i(kna-\omega t)} = -K[2 - e^{-ika} - e^{ika}]e^{i(kna-\omega t)}. \quad (6)$$

Euler's formulas (subtraction) can be used to simplify equation 6 to a more manageable and graphing friendly result. The Euler subtraction is shown below:

$$\begin{aligned} e^{ix} &= \cos x + i \sin x \\ -e^{-ix} &= \cos x - i \sin x \Rightarrow 2 \cos x = e^{-ix} + e^{ix} \\ \cos x + \cos x - e^{-ix} &= e^{ix} \\ \therefore -K[2 - e^{-ika} - e^{ika}] &\Rightarrow -2K[1 - \cos ka]. \end{aligned}$$

Using the simplification in equation 6,

$$\begin{aligned} -M\omega^2 e^{i(kna-\omega t)} &= -2K(1 - \cos ka)e^{i(kna-\omega t)}, \\ -M\omega^2 &= -2K(1 - \cos ka), \\ \omega(k) &= \sqrt{\frac{2K(1 - \cos ka)}{M}}. \end{aligned} \quad (7)$$

The final equation of the dispersion curve frequency as a function of the wave vector k is shown by equation 8; it is found with the half angle to further simplify result in equation 7:

$$\begin{aligned} \sin^2 x &= \frac{1 - \cos(2x)}{2} \Rightarrow 2 \sin^2 \left(\frac{1}{2}x \right) = 1 - \cos x, \\ \therefore \omega(k) &= \sqrt{\frac{2K(1 - \cos ka)}{M}} \Rightarrow \sqrt{\frac{2K \left(2 \sin^2 \frac{1}{2}ka \right)}{M}}, \\ \omega(k) &= 2 \sqrt{\frac{K}{M}} \left| \sin \frac{1}{2}ka \right|. \end{aligned} \quad (8)$$

Solutions describing the actual displacement of the ions are given by the real or imaginary parts of equation 4, i.e.,

$$u(na, t) \propto \begin{cases} \cos(kna - \omega t) \\ \sin(kna - \omega t) \end{cases}. \quad (9)$$

4.2 Normal Modes of a One-Dimensional Lattice with a Basis

The normal mode calculation of a 1-D lattice with a basis is very similar to the monatomic procedure. The representation in figure 11 shows the physical schematic as well as the spring-mass chain visualization. The ions all have the same mass, M. In this crystal structure, there are two equilibrium positions, na and $na+d$, for the ion and its basis, respectively. It is assumed that only the closest neighbors interact.

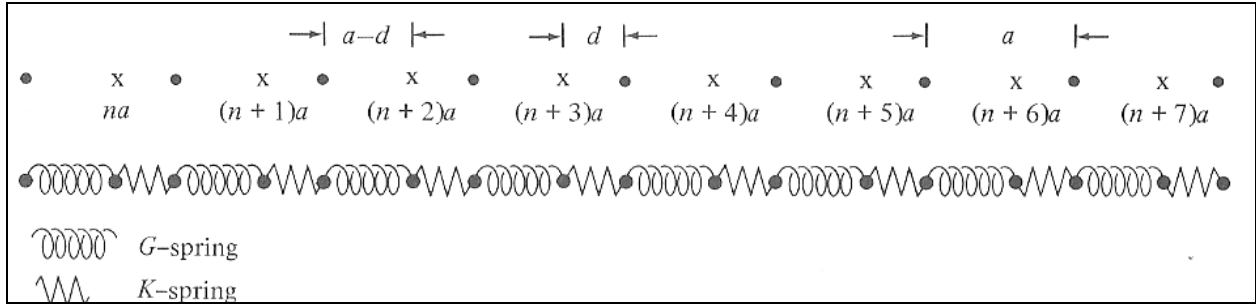


Figure 11. Representation of a 1-D chain with a basis (11).

The spring-mass chain representation can be expressed mathematically as

$$U = \frac{1}{2}k_1x_1^2 + \frac{1}{2}k_2x_2^2.$$

The potential energy is equal to the spring constant and the ion displacement. For the lattice with a basis, both ions must be accounted for and because of the difference in separation distances, the different spring constants and displacements must be recognized.

$$\begin{aligned} k_1 &= K; \quad k_2 = G, \\ x_1 &= u_1(na) - u_2(na), \\ x_2 &= u_2(na) - u_1([n+1]a), \end{aligned}$$

$-u_1(na)$ is the displacement of ion oscillating around site na ,
 $-u_2(na)$ is the displacement of ion oscillating around site $na+d$.

As before, the spring constant k is replaced with K , $G=\varphi''(a)$, where $\varphi(x)$ represents the interaction energy of two ions at distance x apart along the line (spring constant). This interaction energy is found with the Lennard-Jones potential (appendix A). These substitutions give the harmonic potential energy equation as the summation over all ions in the chain:

$$U^{harm} = \frac{K}{2} \sum_n [u_1(na) - u_2(na)]^2 + \frac{G}{2} \sum_n [u_2(na) - u_1([n+1]a)]^2.$$

From the harmonic potential energy equation, the equations of motion can be found if we take the second derivative:

$$\begin{aligned} M\ddot{u}_1(na) &= -\frac{\partial U^{harm}}{\partial u_1(na)} \\ &= -K[u_1(na) - u_2(na)] - G[u_1(na) - u_2([n-1]a)], \\ M\ddot{u}_2(na) &= -\frac{\partial U^{harm}}{\partial u_2(na)} \\ &= -K[u_2(na) - u_1(na)] - G[u_2(na) - u_1([n+1]a)]. \end{aligned}$$

There will be two solutions to the motion system of equations. This is because there will be two modes for the ion and its basis. They can be oscillating at different frequencies about their respective equilibrium positions. These solutions will take the form

$$\begin{aligned} u_1(na) &= \varepsilon_1 e^{i(kna-\omega t)}, \\ u_2(na) &= \varepsilon_2 e^{i(kna-\omega t)}. \end{aligned}$$

The values of ε_1 and ε_2 are ratios that will specify the relative amplitude and phase of vibration of the ions within each lattice cell (11). The same boundary conditions used for the 1-D monatomic chain are used again to retrieve solutions from the equations of motion. Substituting the solution equations into the equations of motion produces two coupled equations by canceling the common exponential factor, leading to

$$\begin{aligned} [M\omega^2 - (K + G)]\varepsilon_1 + (K + Ge^{-ika})\varepsilon_2 &= 0, \text{ and} \\ (K + Ge^{ika})\varepsilon_1 + [M\omega^2 - (K + G)]\varepsilon_2 &= 0. \end{aligned}$$

The homogeneous equations will have a solution, provided the determinant of the coefficients vanishes, leaving

$$[M\omega^2 - (K + G)]^2 = |K + Ge^{-ika}|^2 = K^2 + G^2 + 2KG \cos ka.$$

This equation is satisfied by two positive values of ω . These two values correspond to two different modes on the dispersion diagram and are found from the roots of

$$\omega^2 = \frac{K + G}{M} \pm \frac{1}{M} \sqrt{K^2 + G^2 + 2KG \cos ka}.$$

4.3 One-Dimensional MATLAB Results

The MATLAB code can be modified to find the 1-D phonon normal modes for a monatomic chain as well as a chain with a basis. The code in appendix B solves for the 1-D normal modes. In that code, the two solutions to ω (ion oscillation frequency) can be seen in the wave vector loop. Including both of those equations gives the solution for a 1-D chain with a basis (see figure 12). If one of the equations is removed, the dispersion curve shows the normal mode for a 1-D chain

without a basis (see figure 13). The dispersion relations are symmetric about the zero wave vector. As mentioned in the derivation for the code in section 4.1, the wave vectors from $-\pi/a$ to π/a generate the entire curve for the dispersion relation. The curve would simply be repeated if a larger range of k were graphed. At small values of the wave vector, the relation is linear; the wave vector is short enough to be comparable to the particle spacing; thus, the linearity ceases and the dispersion curve flattens as the group velocity tends to zero (II). The group velocity is the velocity at which the change in the shape of the wave's amplitude propagates through a medium (I). This corresponds to the slope of the dispersion curve.

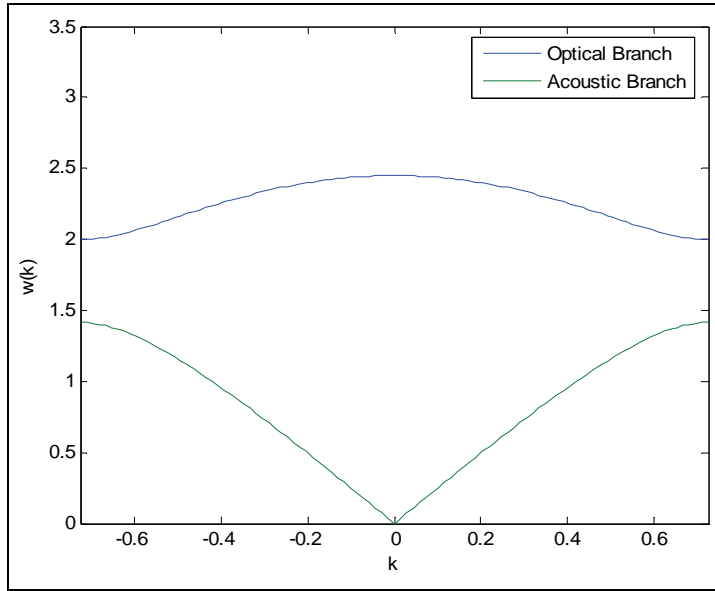


Figure 12. Dispersion curve for a 1-D chain with a basis.

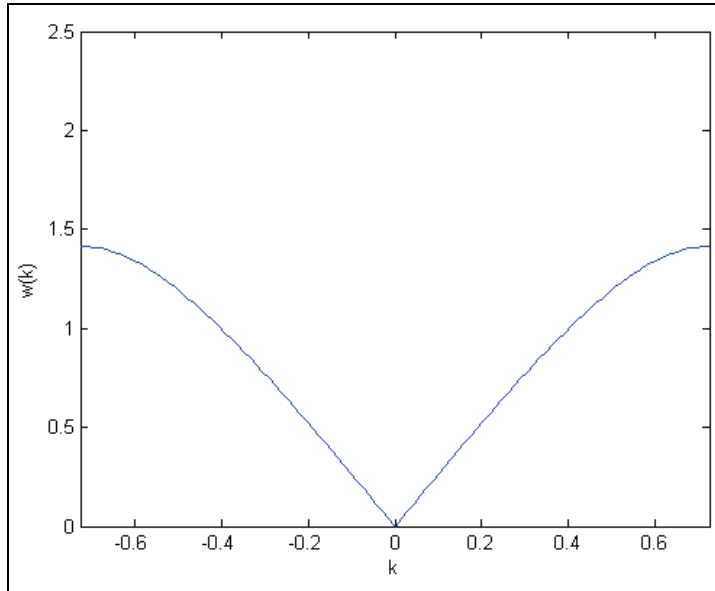


Figure 13. Dispersion curve for a monatomic 1-D chain.

The two functions of frequency, ω , are known as the two branches of the dispersion relation (11). The lower branch is known as the acoustic branch because its dispersion curve is in a form similar to sound waves. The upper branch is referred to as the optical branch because the longer wavelength optical modes in crystals can interact with electromagnetic radiation. The longer wavelength modes are also responsible for the optical characteristics of the crystal (11).

Figure 14 shows the vibration of the ions in the 1-D chain with a basis for the acoustic and optical branch. If the wave vector is taken to be zero, the frequency is equal to zero. This causes the ion and basis to have the same amplitude and phase. The pair moves in phase as the acoustic mode (2). For the optical mode, the ion and its basis move at the same amplitude but out of phase; this results in the pair's center of mass remaining constant. This optical mode occurs with a frequency of vibration in the infrared region, thus the optical branch label.

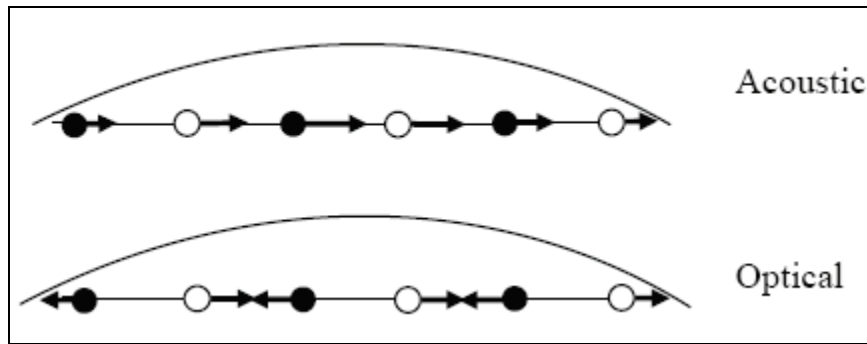


Figure 14. Ion motion during different vibration modes (12).

4.4 Normal Modes of a Two-Dimensional Monatomic Lattice

To calculate the normal modes of a 2-D lattice, the methods for the 1-D chain were modified and expanded. We accomplished this by taking the planar lattice as a mesh of three chains: a horizontal, a vertical, and a diagonal. As shown in figure 15, the lattice has an arbitrary spacing of a , b , and the diagonal distance in which those result. For simplicity, the lattice is made to be monatomic. The l and n variables serve as counters to designate which ion in the lattice is being used.

Applying these three chains results in an equation for the potential energy, given by

$$U = \underbrace{\frac{1}{2} K \sum_l [u_{l,n} - u_{l+1,n}]^2}_{\text{Nearest Neighbors}} + \underbrace{\frac{1}{2} G \sum_n [u_{l,n} - u_{l,n+1}]^2}_{\text{Nearest Neighbors}} + H \underbrace{\sum_l \sum_n [u_{l,n} - u_{l+1,n+1}]^2}_{\text{Next Nearest Neighbors}} .$$

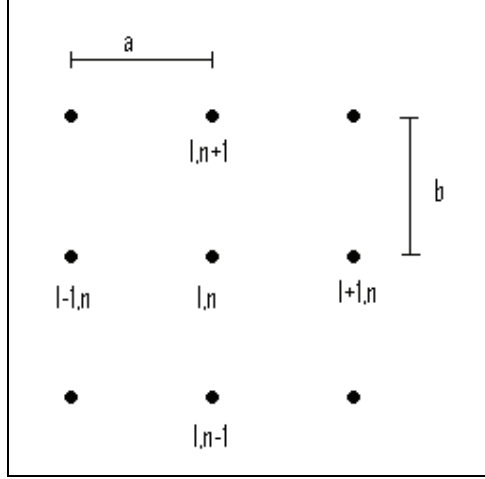


Figure 15. Representation of a 2-D monatomic lattice.

As before, we find the equation of motion for the transverse modes through the medium by taking the second derivative of the potential energy equation. K, G, and H are the three “spring constants” or interaction energy between the ions. These values were found with the Lennard-Jones potential. For the 2-D modes, we made the calculation more accurate by also looking at the next closest neighbors for the interaction energy. If the lattice spacing constants a and b are equal (square lattice), the values of K and G will be the same because of the monatomic stipulation. The resulting equation of motion is

$$M\ddot{u}_{l,n} = -K[2u_{l,n} - u_{l-1,n} - u_{l+1,n}] - G[2u_{l,n} - u_{l,n-1} - u_{l,n+1}] - 2H[2u_{l,n} - u_{l-1,n-1} - u_{l+1,n+1}].$$

With a monatomic lattice, there is only one solution form to satisfy the equation of motion, which is

$$u_{l,n} = e^{i(k_x l a + k_y n b - \omega t)}.$$

Substituting the solution into the equations of motion and solving for the frequency, ω is shown below:

$$\begin{aligned} \omega^2 M &= -K[2 - e^{-ik_x a} - e^{ik_x a}] - G[2 - e^{-ik_y b} - e^{ik_y b}] - 2H[2 - e^{-i(k_x a + k_y b)} - e^{i(k_x a + k_y b)}] \\ \omega^2 M &= -2K[1 - \cos(k_x a)] - 2G[1 - \cos(k_y b)] - 4H[1 - \cos(k_x a + k_y b)] \\ \omega &= \sqrt{-\frac{2}{M} [K(1 - \cos(k_x a)) + G(1 - \cos(k_y b)) + 2H(1 - \cos(k_x a + k_y b))]} \end{aligned}$$

The resulting normal mode equation is

$$\omega = 2\sqrt{\frac{K}{M}} \left| \sin \frac{1}{2} k_x a \right| + 2\sqrt{\frac{G}{M}} \left| \sin \frac{1}{2} k_y b \right| + 4\sqrt{\frac{H}{M}} \left| \sin \left(\frac{1}{2} k_x a + k_y b \right) \right|.$$

With the 2-D planar lattice, it is possible to have wave vectors in multiple directions as opposed to the 1-D chain which could only support a wave vector in the chain's direction. These allowable wave vectors are

$$\vec{k} = \frac{2\pi}{a} \frac{l}{L} \hat{x} + \frac{2\pi}{b} \frac{n}{N} \hat{y}; \quad l, n = 0, \pm 1, \pm 2, \dots, \pm \frac{L, N}{2}$$

4.5 Two-Dimensional MATLAB Results

The MATLAB code for the 2-D planar lattice, as shown in appendix C, was more complicated than the 1-D chain. The main complexity came from the wave vector consideration. In a 1-D chain, the only possible wave vector is the vector traveling through the chain. In the 2-D plane, there may exist horizontal, vertical, and diagonal wave vectors. Figure 16 depicts the dispersion relation for a wave vector with only a horizontal component (the vertical wave vector component was set to zero).

$$k_x = 0$$

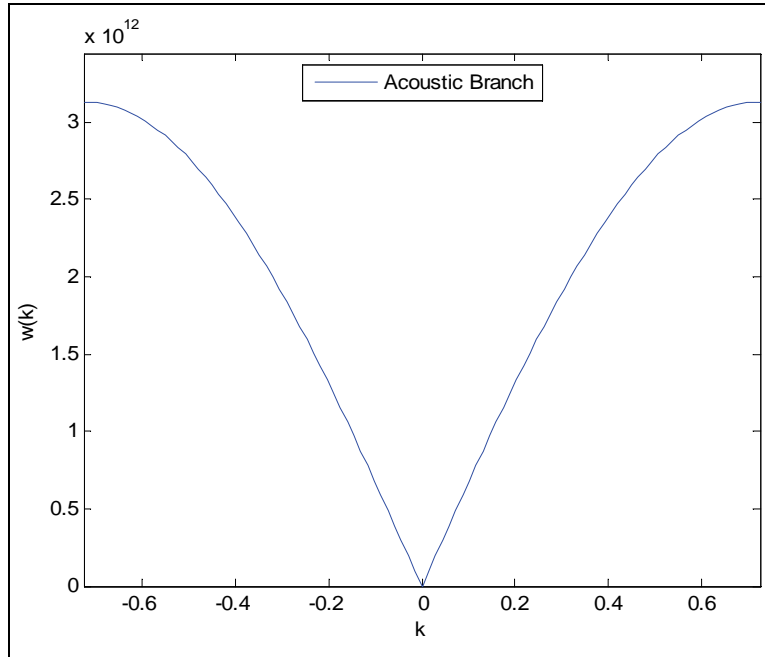


Figure 16. Dispersion curve for a 2-D lattice. (The wave vector is only in the horizontal direction.)

In figure 17, the horizontal and vertical wave vector components were set to equal each other so the wave travels diagonally through the planar lattice. This results in a 3-D graph since the dispersion relation has components in the vertical and horizontal.

$$k_x = k_y$$

In figures 16 and 17, it is clear that the depicted dispersion relation only has an acoustic mode. These curves are very similar to what was seen with the 1-D monatomic chain. With the planar lattice consisting of only a single type of ion, it is expected there would be no optical mode. If

another ion were introduced into the lattice or a basis were added to each lattice point, an optical branch would appear in the dispersion relation.

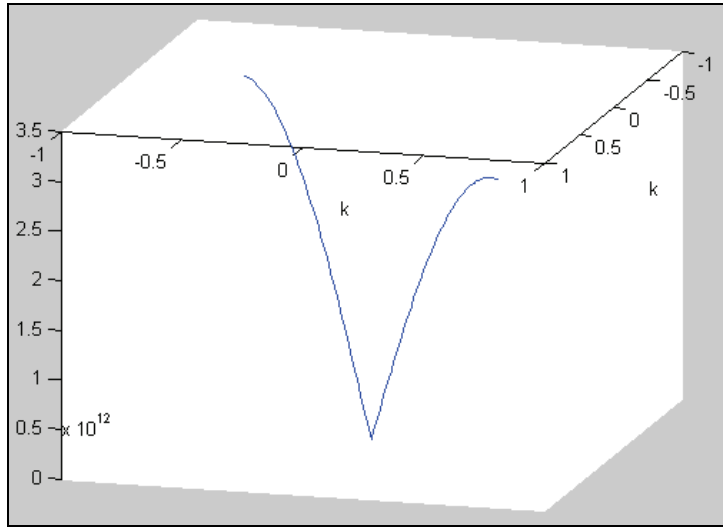


Figure 17. Dispersion curve for a 2-D lattice. (The wave vector is diagonal.)

5. Massachusetts Institute of Technology (MIT) Photonic Bands

The MIT photonic bands (MPB) package is a Unix³-based program for computing band structures of periodic structures. The package was developed by Steven G. Johnson and the Joannopoulos Ab Initio Physics group at MIT. The program computes the eigenstates (harmonic modes) of Maxwell's equations in periodic structures, given arbitrary wave vectors (13). The program uses vector-based math and 3-D analytical methods.

The program is a large step above the MATLAB code introduced in the previous section. It was a logical step in the research progression; the MPB package works well with photonic crystals whereas the MATLAB code was only applicable to phonon mode calculations. The MPB package can accept a wide range of periodic structures and calculates the corresponding dispersion relations.

The MPB package runs a set of provided specifications that are set in a control file. The control files are formatted text documents of the form “*.ctl”. These control files set the geometry of the structure, the number of eigenvectors to compute, what values and information to output, and any other important specifications. When run, the control file activates and accesses a library (libctl) of programming commands that tell the MPB program what to compute. This allows the creation of the control files to be very simple. To run the MPB program, a command such as the following is typed in the Unix prompt:

³Unix is a registered trademark of The Open Group.

```
unix% mpb *.ctl >& *.out
```

This command tells the MPB program to run the *.ctl file and output the results in the *.out file. This *.out file is a readable text file that will provide the results of the calculations the program has run. Several commands that can be invoked at the prompt provide specific information contained in the *.out without the user opening the whole document.

- unix% grep Gap *.out

This command will provide any band gaps in the computed *.out file. It is important to note that any gaps < 1% are most likely attributable to band crossings and are not true band gaps; they have been shown in red in the sample output below.

```
Gap from band 1 (0.275065617068082) to band 2 (0.446289918847647), 47.4729292989213%
Gap from band 3 (0.563582903703468) to band 4 (0.593059066215511), 5.0968516236891%
Gap from band 4 (0.791161222813268) to band 5 (0.792042731370125), 0.111357548663006%
Gap from band 5 (0.838730315053238) to band 6 (0.840305955160638), 0.187683867865441%
Gap from band 6 (0.869285340346465) to band 7 (0.873496724070656), 0.483294361375001%
Gap from band 4 (0.821658212109559) to band 5 (0.864454087942874), 5.07627823271133%
```

- unix% grep tmfreqs *.out > *.tm.dat
unix% grep tefreqs *.out > *.te.dat

This pair of commands takes the TE and TM bands from the *.out output file and organizes the band data into a uniform list. This makes it very easy to take the band structure data and use it for whatever is desired. A sample *.te.dat file is shown below.

```
tefreqs:, 1, 0, 0, 0, 0, 1, 1, 1, 1.41421, 1.41421, 1.41421
tefreqs:, 2, 0.1, 0, 0, 0.1, 0.1, 0.9, 1.00499, 1.00499, 1.1, 1.34536, 1.34536, 1.48661
tefreqs:, 3, 0.2, 0, 0, 0.2, 0.2, 0.8, 1.0198, 1.0198, 1.2, 1.28062, 1.28062, 1.56205
tefreqs:, 4, 0.3, 0, 0, 0.3, 0.3, 0.7, 1.04403, 1.04403, 1.22066, 1.22066, 1.3, 1.64012
tefreqs:, 5, 0.4, 0, 0, 0.4, 0.4, 0.6, 1.07703, 1.07703, 1.16619, 1.16619, 1.4, 1.72047
tefreqs:, 6, 0.5, 0, 0, 0.5, 0.5, 0.5, 1.11803, 1.11803, 1.11803, 1.11803, 1.5, 1.80278
tefreqs:, 7, 0.5, 0.1, 0, 0.509902, 0.509902, 0.509902, 0.509902, 1.02956, 1.02956, 1.2083, 1.2083, 1.50333, 1.74929
tefreqs:, 8, 0.5, 0.2, 0, 0.538516, 0.538516, 0.538516, 0.538518, 0.943398, 0.943399, 1.3, 1.3, 1.51327, 1.7
tefreqs:, 9, 0.5, 0.3, 0, 0.583095, 0.583095, 0.583095, 0.860233, 0.860233, 1.39284, 1.39284, 1.52971, 1.52971
tefreqs:, 10, 0.5, 0.4, 0, 0.640312, 0.640312, 0.640312, 0.781025, 0.781025, 1.48661, 1.48661, 1.55242, 1.55242
tefreqs:, 11, 0.5, 0.5, 0, 0.707107, 0.707107, 0.707107, 0.707107, 0.707107, 1.58114, 1.58114, 1.58114, 1.58114
tefreqs:, 12, 0.4, 0.4, 0, 0.565685, 0.565685, 0.565685, 0.72111, 0.72111, 0.848528, 1.45602, 1.45602, 1.52315, 1.64924
tefreqs:, 13, 0.3, 0.3, 0, 0.424264, 0.424264, 0.424264, 0.762898, 0.762898, 0.763656, 0.990966, 1.33459, 1.33459, 1.47686, 1.72306
tefreqs:, 14, 0.2, 0.2, 0, 0.282843, 0.282843, 0.282843, 0.824621, 0.824621, 1.13137, 1.21655, 1.21655, 1.44222, 1.44222
tefreqs:, 15, 0.1, 0.1, 0, 0.141421, 0.141421, 0.141421, 0.905539, 0.905539, 1.10454, 1.10454, 1.27279, 1.42127, 1.42127
tefreqs:, 16, 0, 0, 0, 0, 0, 1, 1, 1, 1.41421, 1.41421, 1.41421
```

The following three sections demonstrate just a small sample of the capabilities of the MPB program. Sections 5.1 and 5.2 show the analyses of a diamond and tri-rod structure, respectively. Section 5.3 shows how a new structure can be defined and analyzed with the control file.

To construct graphs from the output files (*.out), the following procedure was followed. It is important to note that all the steps can be done with Unix-based programs, but for ease of use, the data were brought into the Windows⁴ OS for manipulation.

1. Run the following to create an output file containing the data for the desired periodic structure:
unix% mpb *.ctl >& *.out
2. Run the following to organize the output file data into a manageable format:
unix% grep tmfreqs *.out > *.tm.dat
unix% grep tefreqs *.out > *.te.dat
3. With Excel⁵ the data can be imported from the *.dat file into the spreadsheet. It is crucial in this step to use comma delimitation to have the data organized in the spreadsheet to greatly accelerate the graphing process.
4. In Excel, the data can be easily graphed and analyzed.

5.1 Diamond Structure

The MPB package came with a folder of sample structures. This folder contained the control files for a range of different periodic structures to demonstrate the MPB software's capabilities. The on-line MPB tutorial (13) provides a walk-through of the diamond structure control file; the walk-through is covered in this section. The diamond control file (diamond.ctl) sets up the periodic structure of a 3-D diamond lattice of dielectric spheres in air. A 3-D model of this structure is shown in figure 18. The control file is given in appendix D. This structure and corresponding full band gap were first introduced by Ho, Chan, and Soukoulis (14).

We calculated the bands by running the following command:

```
unix% mpb diamond.ctl >& diamond.out
```

Based on Ho, Chan, and Soukoulis (14), a full band gap should exist in the band structure. This is explored by the following command:

```
unix% grep Gap diamond.out
Gap from band 2 (0.396348703007373) to band 3 (0.440813418580596), 10.6227251392791%
```

This output shows that there is a 10.6% band gap from band 2 to band 3. This gap can be seen in figure 19 from the tutorial and figure 20 which was generated with Excel to graph the MPB output data. Figures 18 and 19 are identical, which verifies that the MPB code and resulting data files were used correctly. Figure 19 also matches a figure from the paper (14). The figure from the paper was generated by other means; it is encouraging that it matches the MPB output.

⁴Windows is a trademark of Microsoft Corporation.

⁵Excel is a trademark of Microsoft Corporation.

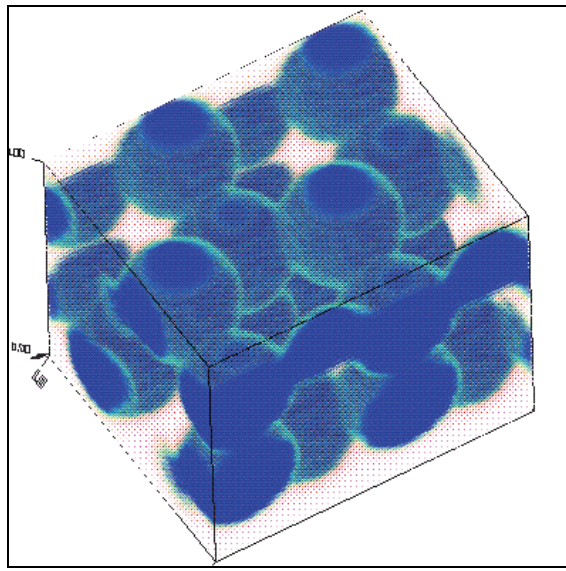


Figure 18. Diamond structure depiction (13) (MIT photonic-band tutorial figure).

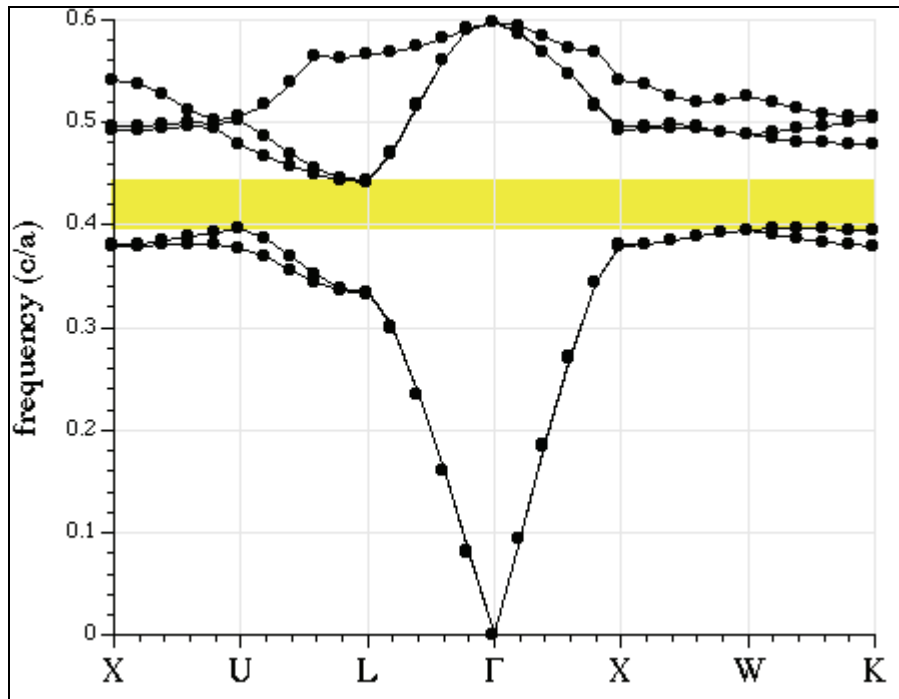


Figure 19. Diamond band diagram (14) (MIT photonic-band tutorial figure).

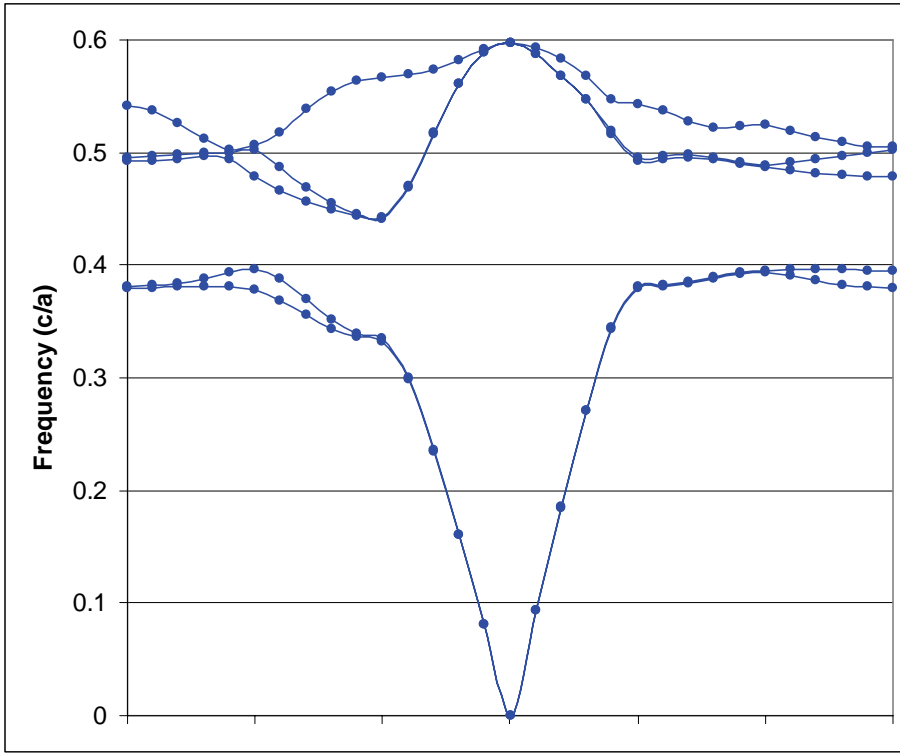


Figure 20. Diamond band diagram (MIT photonic-band program generated plot).

5.2 Tri-rods Structure

The second periodic structure MPB example that was covered in the on-line MPB tutorial (13) was the tri-rods structure control file (tri-rods.ctl). The walk-through from the on-line tutorial is covered in this section. The structure is a 2-D triangular lattice of dielectric rods (figure 19). The control file, tri-rods.ctl is shown in appendix E.

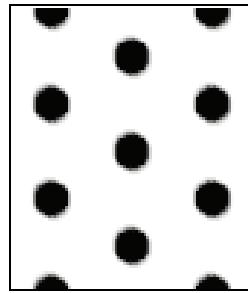


Figure 21. Rods in a triangular lattice (13), top view.

We calculated the bands by running the following command:

```
unix% mpb tri-rods.ctl >& tri-rods.out
```

The band gaps were verified with the following command:

```
unix% grep Gap tri-rods.out
```

Gap from band 1 (0.275065617068082) to band 2 (0.446289918847647), 47.4729292989213%

Gap from band 3 (0.563582903703468) to band 4 (0.593059066215511), 5.0968516236891%

Gap from band 4 (0.791161222813268) to band 5 (0.792042731370125), 0.111357548663006%

Gap from band 5 (0.838730315053238) to band 6 (0.840305955160638), 0.187683867865441%

Gap from band 6 (0.869285340346465) to band 7 (0.873496724070656), 0.483294361375001%

Gap from band 4 (0.821658212109559) to band 5 (0.864454087942874), 5.07627823271133%

The gaps in red are less than 1% and are therefore bands crossing one another. The other three bands are significant in size and can be seen on the band structure diagram (see figure 22). It is important to note that unlike the diamond structure, there is no complete band gap. There are only partial TE and TM band gaps. In figure 22, the light blue area represents TM band gaps and the light red represents the TE band gap.

Figure 23 shows the Excel graph generated from the output (tri-rods.*.dat). It can be seen that the band structure in figure 23 identically matches the band structure diagram in figure 22 from the online MPB tutorial.

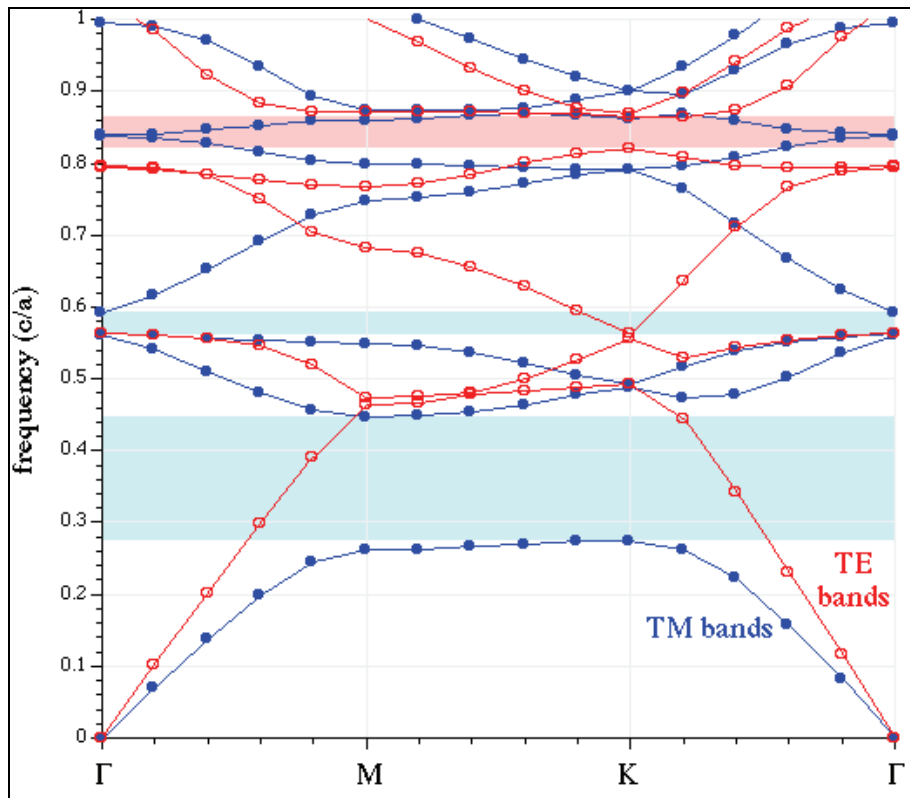


Figure 22. Tri-rods band diagram (13) (MIT photonic band tutorial figure).

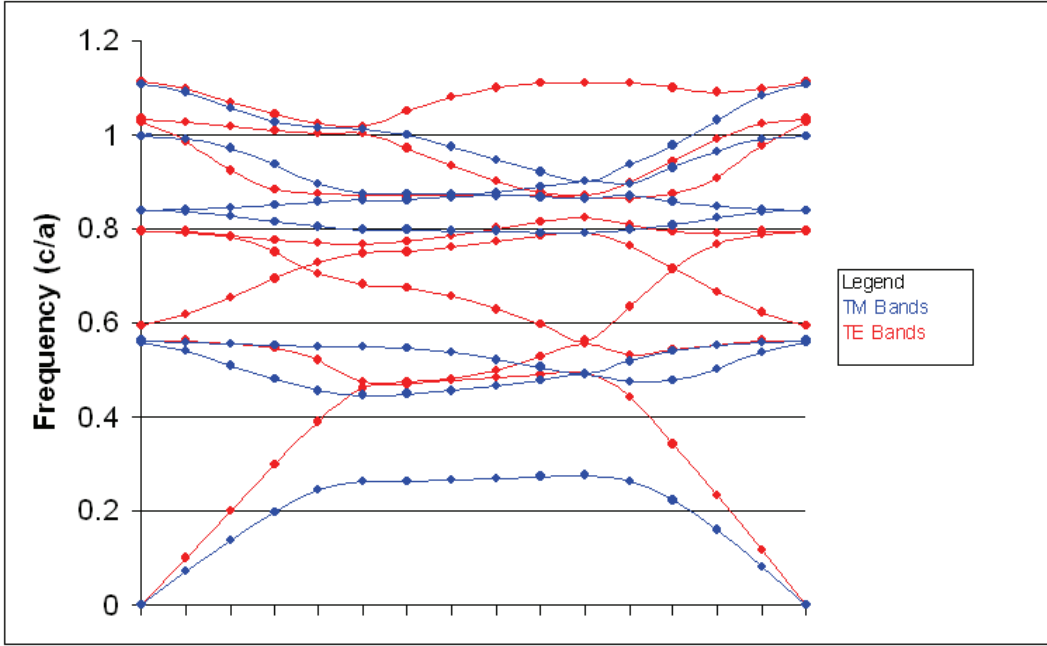


Figure 23. Tri-rods band diagram (MIT photonic band program-generated plot).

5.3 Sample Structure

After the two examples are complete, the on-line MPB tutorial (13) shows how to create a control file. This is shown in the user tutorial section. After one becomes familiar with the basic commands through the user tutorial, the user reference section on line (13) can be used to further explore commands that can be used in the control file. To test the program and control file function, a sample structure was developed and run. The sample control file (sample.ctl) is shown in figure 24. The control file is very short and concise. This is part of the advantage of the library (libctl) discussed before. It allows short commands such as "set! *" to call up a longer code in the library that the MPB program then executes. The sample structure is a 3-D cube of dielectric material with an air hole at its center.

We calculated the bands for the sample structure by running the following command:

```
unix% mpb sample.ctl >& sample.out
```

To look at the band gap, the familiar "unix% grep Gap sample.out" was used, but no output was provided. This is because there are no partial or full band gaps in the structure. This is evident in the band diagram in figure 25.

```

(set! num-bands 8)

(set! k-points (list (vector3 0 0 0) ; Gamma
(vector3 0.5 0 0) ; X
(vector3 0.5 0.5 0) ; M
(vector3 0 0 0))) ; Gamma

(set! k-points (interpolate 4 k-points))

; A unit cube of dielectric material with a spherical air hole of radius 0.2 at
; its center,

(set! geometry (list
(make block (center 1 2 3) (material (make dielectric (epsilon 12))) (size 1 1 1))
(make sphere (center 1 2 3) (material air) (radius 0.2)))))

(set! geometry-lattice (make lattice (size 1 1 no-size)))

(set! resolution 32)

(run-tm)
(run-te)

```

Figure 24. Sample control file for MPB.

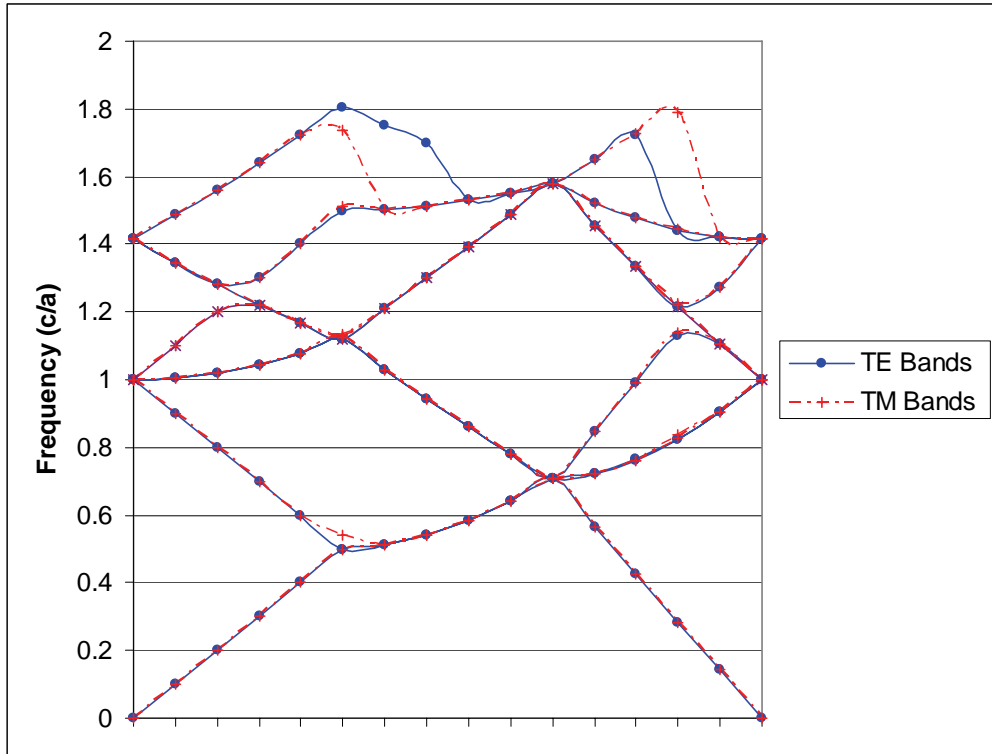


Figure 25. Sample band structure (MIT photonic band program-generated plot).

5.4 MIT Photonic-Bands Conclusion

The MPB package is a powerful program to use in the study of photonic crystals. After the preliminary study of the background of photonics and photonic crystals, the program's capabilities are easy to appreciate. The ability to specify the geometry of periodic structures with easy commands in the control file allows for the fast study of different structures. The MPB program is useful as a concept evaluator to analyze and predict the band structures of conceived designs through computational modeling before we perform physical experiments.

The MPB package proved to be a useful educational tool. The control file feature allows the program to be very user friendly. The basic commands used in the control file can be quickly learned from the on-line tutorial and user reference, leading to immediate results of photonic properties of materials.

7. References

1. Pedrotti, Frank. *Introduction to Optics*; Pearson Prentice Hall: New Jersey, 2007.
2. Johnson, S. G.; Joannopoulos, J. D. *Introduction to Photonics: Bloch's Theorem, Band Diagrams, and Gaps*. The Joannopoulos Research Group at MIT, 28 March 2007, web site: <<http://ab-initio.mit.edu/photons/>>.
3. Web site: <https://netfiles.uiuc.edu/pruzinsk/www/research_intro.htm>.
4. The Joannopoulos Research Group at MIT. *Photonic Crystals Tutorial Lectures 1-5*, 28 March 2007, web site: <<http://ab-initio.mit.edu/photons/>>.
5. Web site: <<http://msc.phys.rug.nl/compphys0/>>.
6. Yablonovitch, Eli. Photonic Crystals: Semiconductors of Light. *Scientific American December 2001*, 47-55.
7. Web site: <<http://www.bergen.org/istf/02-598/comp1.html>>.
8. El-Kady, I.; Reba Taha, M. Nano Photonic Sensors for Microdamage Detection: An Exploratory Simulation. *2005 IEEE International Conference on Systems, Man and Cybernetics 2005*, 2, 1961-1966.
9. Park, W.; Lee, J.-B. Mechanically Tunable Photonic Crystal Structure. *Applied Physics Letters 2004*, 85, 4845.
10. Jacobsen, R. S. Strained Silicon as a New Electro-Optic Material. *Nature 441 2006*, 199-202.
11. Kittel, Charles. *Solid State Physics*; 7th ed., Wiley: New York, 1995.
12. Tsymbal, E. Y. *Physics 927: Introduction to Solid State Physics Course Lectures 1-5*, web site: <http://physics.unl.edu/~tsymbal/tsymbal_files/Teaching/SSP927/Section%2005_Lattice_Vibrations.pdf>.
13. Steven Johnson and Joannopoulos Ab Initio Physics Group at MIT. *MIT Photonic-Bands Program*, 28 March 2007, web site: <http://ab-initio.mit.edu/wiki/index.php/MIT_Photonic_Bands>.
14. Ho, K. M.; Chan, C. T.; Soukoulis, C. M. Existence of a Photonic Gap in Periodic Dielectric Structures. *Physical Review Letters 1990*, 65, 3152.

Appendix A. Lennard-Jones Potential

The Lennard-Jones potential is a mathematical formula that approximates the interaction energy between two ions, based on their radius of separation r . As seen in figure A-1, at close range, there is a repulsive energy that goes to infinity. Farther away, there is an attractive force that tends toward zero as the radius of separation is increased. In the derivation below, $\Phi(r)$ is the value of the interaction potential. The derivative of $\Phi(r)$ is taken twice to find the “spring constant” or interaction energy between two ions. This interaction energy was used in the normal phonon mode derivations and MATLAB programs.

$$\begin{aligned}\phi''(r) &= K, G, H \\ r &= a, b, \sqrt{a^2 + b^2} \\ \phi(r) &= 4\epsilon \left[\left(\frac{\sigma}{r}\right)^{12} - \left(\frac{\sigma}{r}\right)^6 \right] \\ \phi(r) &= 4\epsilon \left[\sigma^{12} \left(\frac{1}{r^{12}}\right) - \sigma^6 \left(\frac{1}{r^6}\right) \right] \\ \frac{d\phi(r)}{dr} &= 4\epsilon \left[-12\sigma^{12} \left(\frac{1}{r^{13}}\right) + 6\sigma^6 \left(\frac{1}{r^7}\right) \right] \\ \frac{d^2\phi(r)}{dr^2} &= \phi''(r) = 8\epsilon \left[\left(\frac{78\sigma^{12}}{r^{14}}\right) - \left(\frac{21\sigma^6}{r^8}\right) \right]\end{aligned}$$

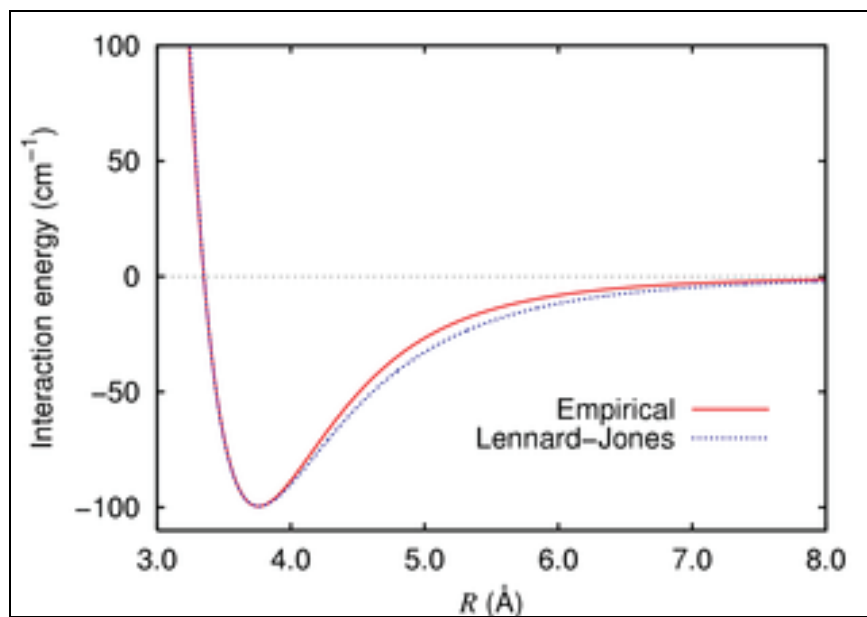


Figure A-1. Lennard-Jones potential. (The graph shows how closely the Lennard-Jones potential fits the empirical curve for argon atoms. The x-axis is the radius of separation in angstroms [1].)

Appendix B. MATLAB Code: Dispersion Curves for One-Dimensional Lattice

```
clear all
clc
%function omega = dispersion(phi)
syms L N omega k kx ky a b K G M

%Test Input
L=10;
N=10;
a=4.33;
b=20;
K=1;
G=2;
M=1;

j=1;
%Set loop to cover entire lattice
e=-N/2;
r=N/2;
for i = e:.1:r
    %Wave vector
    kx(j)=(2*pi()/a)*(i/L);
    %Dispersion Curve Equation
    omega1(j) = sqrt(((K+G)/M)+(1/M)*sqrt(K^2+G^2+2*K*G*cos(kx(j)*a)));
    omega2(j) = sqrt(((K+G)/M)-(1/M)*sqrt(K^2+G^2+2*K*G*cos(kx(j)*a)));
    j=j+1;
end
kx=double(kx);
omega1=double(omega1);
omega2=double(omega2);
plot(kx, omega1, kx, omega2)
legend('Optical Branch','Acoustic Branch','Location','NorthEast')
xlabel('k')
ylabel('w(k)')
axis([-pi()/a pi()/a 0 3.5])
```

INTENTIONALLY LEFT BLANK

Appendix C. MATLAB Code: Two-Dimensional Phonon Dispersion Curve

```
function Dispersion2D(epsilon, sigma, r, m)
%Phonon Dispersion Curves for Two-Dimensional Monatomic Lattice
%function Dispersion2D(epsilon, sigma, r, m)
%Calcualte Interaction Energy
phi= 8*epsilon*(((78*sigma^12)/(r^14))-((21*sigma^6)/(r^8))...
+8*epsilon*(((78*sigma^12)/((2*r)^14))-((21*sigma^6)/((2*r)^8)))
%Next nearest neighbors addition
%Xenon Test Inputs
%epsilon=0.02;
%sigma=3.98;
%r=4.33;
%m=131.29
syms L N omega k kx ky a b K G M
%Input for Monatomic Homogeneous Lattice:
a=r;
b=r;
K=phi;
G=phi;
M=m*1.66053886e-27; %convert amu to kg
%Lattice Size:
L=10; N=10;
%Set loop to cover entire lattice
e=N/2;
j=1;
for i = -e:1:e
    kx(j)=(2*pi()/a)*(i/L);
    ky(j)=(2*pi()/b)*(i/N);
    %k(i)=[kx(i), ky(i)];
    %Dispersion Curve Equation
    omega(j) = 2*sqrt(K/M)*abs(sin((1/2)*kx(j)*a))...
    +2*sqrt(G/M)*abs(sin((1/2)*ky(j)*b));
    j=j+1;
end
kx=double(kx);
ky=double(ky);
omega=double(omega);
plot(kx, omega)
xlabel('k')
ylabel('w(k)')
axis([-pi()/a pi()/a 0 1.1*max(omega)])
legend('Acoustic Branch','Location','North')
figure
plot3(kx, ky, omega)
xlabel('k'); ylabel('k'); zlabel('w(k)')
```

INTENTIONALLY LEFT BLANK

Appendix D. Diamond Structure Control File (diamond.ctl)

```
(set! geometry-lattice (make lattice
    (basis-size (sqrt 0.5) (sqrt 0.5) (sqrt 0.5))
    (basis1 0 1 1)
    (basis2 1 0 1)
    (basis3 1 1 0)))

; Corners of the irreducible Brillouin zone for the fcc lattice,
; in a canonical order:
(set! k-points (interpolate 4 (list
    (vector3 0 0.5 0.5) ; X
    (vector3 0 0.625 0.375) ; U
    (vector3 0 0.5 0) ; L
    (vector3 0 0 0) ; Gamma
    (vector3 0 0.5 0.5) ; X
    (vector3 0.25 0.75 0.5) ; W
    (vector3 0.375 0.75 0.375)))) ; K

; define a couple of parameters (which we can set from the command-line)
(define-param eps 11.56) ; the dielectric constant of the spheres
(define-param r 0.25) ; the radius of the spheres

(define diel (make dielectric (epsilon eps)))

; A diamond lattice has two "atoms" per unit cell:
(set! geometry (list (make sphere (center 0.125 0.125 0.125) (radius r)
    (material diel))
    (make sphere (center -0.125 -0.125 -0.125) (radius r)
    (material diel)))))

; (A simple fcc lattice would have only one sphere/object at the origin.)

(set-param! resolution 16) ; use a 16x16x16 grid
(set-param! mesh-size 5)
(set-param! num-bands 5)

; run calculation, outputting electric-field energy density at the U point:
(run (output-at-kpoint (vector3 0 0.625 0.375) output-dpwr))
```

INTENTIONALLY LEFT BLANK

Appendix E. Tri-Rods Structure Control File (tri-rods.ctl)

```
(set! num-bands 8)

(set! geometry-lattice (make lattice (size 1 1 no-size)
                                (basis1 (/ (sqrt 3) 2) 0.5)
                                (basis2 (/ (sqrt 3) 2) -0.5)))
(set! geometry (list (make cylinder
                           (center 0 0 0) (radius 0.2) (height infinity)
                           (material (make dielectric (epsilon 12)))))

(set! k-points (list (vector3 0 0 0) ; Gamma
                      (vector3 0 0.5 0) ; M
                      (vector3 (/ -3) (/ 3) 0) ; K
                      (vector3 0 0 0))) ; Gamma
(set! k-points (interpolate 4 k-points))

(set! resolution 32)

(run-tm (output-at-kpoint (vector3 (/ -3) (/ 3) 0)
                           fix-e-field-phase output-e-field-z))
(run-te)
```

INTENTIONALLY LEFT BLANK

Appendix F. An Introduction to Ferroelectric Fatigue

Introduction

Ferroelectric materials have many applications because of their ability to have spontaneous polarization. They are used in sensors and actuators in addition to dynamic and non-volatile ferroelectric memory devices. Unfortunately, there are several drawbacks to ferroelectric materials. Ferroelectrics have low fracture toughness and can crack easily because of their brittle nature. Another main issue preventing the widespread commercialization of ferroelectric materials is ferroelectric (polarization) fatigue. This is the loss of switchable polarization in a material as a function of the number of switching cycles. A switching cycle is when an applied external electric field is cycled from one direction to the complete opposite. The crack formation and ferroelectric fatigue lead to a loss in performance of the material. Ferroelectric performance is the ability and quickness with which the material can switch polarization. This performance loss generates reliability concerns for devices that use ferroelectrics.

A way to predict ferroelectric fatigue would provide great insight into improving the fatigue life. Fatigue life is the number of cycles until the material fails and can no longer switch polarizations. This would open the door for optimization of ferroelectric materials. One way to accomplish this goal is through the use of a model that can provide fatigue life based on entered parameters. Arias et al.⁶ propose a phenomenological cohesive model of ferroelectric fatigue to predict fatigue life.

Background

A dielectric material is one that is non-conducting. Ferroelectrics are a subset of dielectrics that exhibit interesting properties such as a high dielectric constant. They are materials that are polar by nature. They are polar because ferroelectric crystal cells have a dipole moment even when not subjected to an external electric field. The dipole is a result of different center locations of the positive and negative charges within the crystal cell. Because of the dipole moment, the crystal is said to be polarized, meaning it contains a dipole moment that acts over some volume. Crystals that have spontaneous polarization are called pyroelectric and the polarization occurs along the polar axis. Ferroelectrics have multiple equilibrium states of the spontaneous polarization vector. An applied external electric field can switch the orientation of the spontaneous polarization vector if it is strong enough to overcome the polarization energy barrier.

Ferroelectric materials have a temperature above which they become paraelectric, meaning they no longer are spontaneously polarized. The temperature where this occurs is the Curie point, T_c . Below the Curie temperature, the ferroelectric crystal undergoes a structural phase change. This

⁶Arias, I.; Serebrinsky, S.; Ortiz, M. A Phenomenological Cohesive Model of Ferroelectric Fatigue. *Acta Mater.* 2006, 54 (4), 975-984.

shift of atoms within the cell generates the polarization as well as new unit cell dimensions. The spontaneous polarization does not have to occur uniformly across the whole medium. Multiple polarization vectors can exist across the material. Areas of the same polarization direction are known as ferroelectric domains. The orientation of ferroelectric domains throughout the material is attributable to the mechanical and electrical boundary conditions to which the material is subjected. The domains orient themselves to minimize the surface charge and the elastic energy resultant of mechanical constraints. The surface charge is a result of the onset of spontaneous polarization. This surface charge produces an electric field called a depolarizing field which acts opposite the overall polarization⁷. The area where two domains meet is a domain wall. If the domains are oppositely polarized, it is a 180-degree domain wall. If the domains' polarization vectors are perpendicular to one another, it is a 90-degree domain wall.

A plot of polarizations versus electric field will produce a hysteresis loop. This demonstrates the ability of an electric field to reverse the spontaneous polarization of some or all domains in the material. If the crystal starts with an equal number of opposing domains, its overall polarization is zero. If an electric field is applied, some of the domains opposing the field will reverse. As the field is increased, the domains will continue to switch until a critical point (the state of saturation) is reached. At this point, all domains are oriented in the direction of the field. If the field is decreased, the polarization will not return to zero but will decrease more gradually. When the field is reduced to zero, some of the domains will retain the direction of the first critical state; this is known as remnant polarization, P_r . If an opposite field is applied, the domains will reverse direction until all are oriented with the field at a second opposite state of saturation. The coercive field, E_c , is the electric field required for the polarization to equal zero.

Ferroelectric fatigue is a very complex phenomenon. It is defined as the loss of remnant polarization as a function of the number of switching cycles. In addition to electric field cycling, other factors can decrease the remnant polarization. Several fatigue mechanisms have been identified as causes of ferroelectric fatigue. Domain wall pinning is where space charges or injected charges prevent the movement of domain walls; this mechanism operates mostly in the bulk of the material. Near the electrode interfaces, nucleation of oppositely oriented domains is inhibited. This means that the formation of opposite domains is prevented by space charges produced during electric field cycling. Oxygen vacancies in the crystal could also be a fatigue mechanism. The vacancies could pin domain walls and/or create structural damage at the interface between the ferroelectric and electrode. Micro-cracking is also identified as a cause of polarization loss, although it is a purely mechanical defect. Concentrated stress or electric fields at the crack tip induce local switching that can shield or promote crack growth. Crack growth is affected by electrical conditions at crack faces, by the grain size, and by the porosity of the material⁸. Many

⁷Damjanovic, D. Ferroelectric, Dielectric and Piezoelectric Properties of Ferroelectric Thin Films and Ceramics. *Rep. Prog. Phys.* **1998**, *61* (9), 1267–1324.

⁸Arias, I.; Serebrinsky, S.; Ortiz, M. A Phenomenological Cohesive Model of Ferroelectric Fatigue. *Acta Materialia* **2006**, *54*, 975–984.

fatigue mechanisms may depend on frequency as well as the amplitude of the applied electric field. Ferroelectric fatigue causes the polarization versus electric field hysteretic loop to change shape. After a certain number of cycles corresponding with onset of fatigue, the maximum polarization level or state of saturation decreases. The crystal is no longer able to attain its original maximum polarization.

Cohesive Model

Paris et al.⁹ laid the foundation for fatigue life prediction. The work provided phenomenological laws relating applied stress amplitude to fatigue crack growth rate. The model is known as Paris' Law. The law was ground breaking at the time but was based on the ideal conditions of small yielding, constant stress amplitude and long cracks. If these criteria were not met, the law's prediction capabilities were greatly diminished. Although Paris's law only worked for select cases, it paved the way for future fatigue modeling in materials.

A model using cohesive laws was developed by Nguyen et al.¹⁰ to predict fatigue life based on fatigue crack growth. The model was prepared to predict the fatigue life of metals (aluminum was used for experimental data)). The model augmented Paris' law through the use of cohesive laws. These laws exhibit unloading-loading hysteresis which allows for steady crack growth modeling. Cohesive theories take fracture as a gradual process where incipient material surface separation is resisted by cohesive tractions. The tractions go to zero at a point of critical opening displacement. Previous models used an elastic cycle of fatigue but the cohesive law replaces that with unloading-loading hysteresis. Many of the previous modifications of Paris' law had been *ad hoc*, meaning they were derived from experimental data. The cohesive laws provided a means to create a model that could predict fatigue life before experimental data were taken. The crack growth results from interaction of bulk cycle plasticity, closure, and gradual decohesion at the crack tip. This model was a step in the right direction but no cohesive model existed for ferroelectric materials.

In 2004, Arias et al. developed a model to describe fatigue-crack nucleation and growth for ferroelectric materials subject to electro-mechanical loading. This was the first model based around a hysteretic cohesive law that couples mechanical and electric fields to predict fatigue in ferroelectrics. This was important because ferroelectric materials demonstrate electrical and mechanical fatigue under cyclic electrical loading. The model also could take into account electro-mechanical loading which is what ferroelectrics are subjected to in operation more often than purely mechanical stress as in metals. The cohesive law can be used in tandem with general constitutive relations of bulk behavior to predict fatigue crack growth under arbitrary loading conditions. This model is also able to predict fatigue crack nucleation which the previous crack growth model (2001) could not. This is important for fatigue prediction in smooth-surfaced

⁹Paris, P.C.; Gomez, M.P.; Anderson, W.P. A Rational Analytical Theory of Fatigue. *The Trend in Engineering* **1961**, *13*, 9-14.

¹⁰Nguyen, O.; Repetto, E. A.; Ortiz, M.; Radovitzky, R. A Cohesive Model of Fatigue Crack Growth. *Int. J. Fract.* **2001**, *110* (4), 351–369.

material with no initial cracking. One large benefit of this model is the ability of cohesive theories to apply to arbitrary crack and specimen geometries and loading histories. A shortcoming of the model is that it is phenomenological in nature and some details were chosen because of convenience. We must determine some parameters of the model experimentally by fitting to fatigue data or by measuring parameters individually.

The most recent phenomenological cohesive model of ferroelectric fatigue produced by Arias et al. (2006) is a great advancement in ferroelectric fatigue life prediction. Like the preceding model, it predicts ferroelectric fatigue under electro-mechanical loading through the use of cohesive laws. The revised cohesive law couples mechanical displacement and electric-potential discontinuity to mechanical tractions and surface-charge density. The model applies to fatigue when it is localized in planar surfaces that are treated as cohesive surfaces. The surface is modeled as a ferroelectric material by representing both mechanical opening displacement and electric-potential discontinuity. The cohesive law is extended to represent these and mechanical tractions and surface-charge density as a work-conjugate pair. To retrieve qualitative data, a “Smith-Ferrante monotonic envelope” and an exponential-decay law of loading-unloading hysteresis were used. The model delivers the following:

- Existence of a threshold field for the onset of fatigue,
- Dependence of threshold on the applied field frequency,
- Dependence of fatigue life on the amplitude of the field,
- Dependence of the coercive field on the size of the component (size effect).

To gauge the validity of the system, a simple test configuration provided experimental data to compare to the model output. The test configuration consisted of an “infinite” slab of PZT (lead zirconate titanate $Pb[Zr_xTi_{1-x}]O_3$) acted upon by an oscillatory voltage differential across the slab without other stresses. The results were not conclusive but they did indicate planar-like regions affected by cycling may lead to the observed fatigue in tetragonal PZT.

Conclusion

To accurately determine the interactions between fracture, deformation, and defective structures that cause ferroelectric fatigue, a physics based multi-scale model is needed. This model would be a huge step in predicting the fatigue life of ferroelectric devices. Until that is produced, the current phenomenological model should be improved upon and validated by experiments so it will be useful for future ferroelectric design. Several actions can be taken to improve the current model. The first is to run the same simple test configuration that was done with PZT on different ferroelectric materials. Having more data on multiple materials will aid in the following proposed actions. Extension and calibration of the model could improve data agreement. The results could also optimize fit to the experimental data. Assumptions made in the derivation of the model could be studied further to confirm their validity. Another area of concern is the fact that the model only applies to changes in properties that lead to fatigue in planar regions. A more comprehensive

model working on arbitrary sections of material would be very helpful for specific material application fatigue prediction. Full finite element calculations, more precise bulk material constitutive relations, and the study of the cohesive law aspects of the monotonic envelope and loading-unloading law should be pursued.

Although results were inconclusive for the cohesive model compared to the experimental test configuration, it is crucial to put work into the model to improve it. To have a model that could accurately predict the ferroelectric fatigue effect of an electro-mechanical loading would greatly aid future work with ferroelectric materials such as PZT. The properties of these ferroelectric materials make them crucial in the improvement of current technologies and the implementation of emerging technologies. Fatigue aspects are especially important for the Army where equipment is constantly subjected to harsh and dynamic operating conditions.

<u>NO. OF COPIES</u>	<u>ORGANIZATION</u>	<u>NO. OF COPIES</u>	<u>ORGANIZATION</u>
1 (PDF ONLY)	DEFENSE TECHNICAL INFORMATION CTR DTIC OCA 8725 JOHN J KINGMAN RD STE 0944 FORT BELVOIR VA 22060-6218	6	DIRECTOR US ARMY RSCH LABORATORY ATTN AMSRD ARL CI HC J CLARKE P CHUNG (5 CYS) BLDG 394
1	US ARMY RSRCH DEV & ENGRG CMD SYSTEMS OF SYSTEMS INTEGRATION AMSRD SS T 6000 6TH ST STE 100 FORT BELVOIR VA 22060-5608		
1	DIRECTOR US ARMY RESEARCH LAB IMNE ALC IMS 2800 POWDER MILL RD ADELPHI MD 20783-1197		
1	DIRECTOR US ARMY RESEARCH LAB AMSRD ARL CI OK TL 2800 POWDER MILL RD ADELPHI MD 20783-1197		
2	DIRECTOR US ARMY RESEARCH LAB AMSRD ARL CS OK T 2800 POWDER MILL RD ADELPHI MD 20783-1197		
2	DIRECTOR US ARMY RESEARCH LAB AMSRD ARL CI J GOWENS R NAMBURU 2800 POWDER MILL RD ADELPHI MD 20783-1197		

ABERDEEN PROVING GROUND

- 1 DIRECTOR
US ARMY RSCH LABORATORY
ATTN AMSRD ARL CI OK (TECH LIB)
BLDG 4600
- 1 DIRECTOR
US ARMY RSCH LABORATORY
ATTN AMSRD ARL CI H C NIETUBICZ
BLDG 328